ADVANCED TOPICS SECTION

The Advanced Topics Section is meant for articles that deal with physics more advanced than is typical of regular articles in AJP. Though advanced, these articles have been judged to give clear presentations of material useful to a segment of AJP readers.

Electric field lines of an arbitrarily moving charged particle

S. G. Arutunian[a)]
Alikhanyan National Scientific Laboratory, 0036 Yerevan, Armenia and CANDLE Synchrotron Research Institute, 0040 Yerevan, Armenia

M. A. Aginian and A. V. Margaryan
Alikhanyan National Scientific Laboratory, 0036 Yerevan, Armenia

M. Chung[b)]
Ulsan National Institute of Science and Technology, 44919 Ulsan, South Korea

E. G. Lazareva
Alikhanyan National Scientific Laboratory, 0036 Yerevan, Armenia

(Received 6 September 2022; accepted 16 July 2023)

Electromagnetic fields of relativistic charged particles have a broad frequency spectrum and a sophisticated spatial structure. Field lines offer a visual representation of this spatial structure. In this article, we derive a general set of equations for the field lines of any moving charged particle. The electric field lines are completely determined by the unit vector from the retarding point to the observation point. After proper transformations, the field line equations describe the rotation of this vector with an angular velocity coinciding with Thomas precession. In some cases, including all planar trajectories, the field line equations reduce to linear differential equations with constant coefficients. We present a detailed derivation of these equations and their general analytical solution. We then illustrate this method by constructing field lines for the "figure eight" motion of an electric charge moving under the influence of a plane wave, including complex field lines in three dimensions.
https://doi.org/10.1119/5.0124544

I. INTRODUCTION

Electric field lines provide a way to visualize the radiation of a relativistic particle, giving insight into the structure of the field. To understand the formation of the radiation field, it is useful to observe the field lines, starting from the Coulomb region and extending into the radiation zone.

The present work is motivated by a recent paper in the *American Journal of Physics* that analyzed electromagnetic fields of relativistic point charges by constructing electric field lines.[1] The electromagnetic field of a charge moving along the trajectory $\vec{r}_0(t)$ is derived from the Lienard–Wiechert potentials, in which the retardation equation plays a key role. This equation relates the observation point $\vec{r}$ to a point on the trajectory $\vec{r}_0(t')$ at the retarded time t',

$$t - t' = |\vec{r} - \vec{r}_0(t')|/c, \tag{1}$$

where c is the speed of light. Electrodynamics textbooks often state that the point $\vec{r}_0(t')$ is connected to the point $\vec{r}$ by a "light signal" or "light dot" that originates at the retarded time from the point $\vec{r}_0(t')$ and reaches the point $\vec{r}$ at the observation time.[2–4] Light dots move at the speed of light, and their directions of motion are characterized by a unit vector $\vec{n} = (\vec{r} - \vec{r}_0(t'))/|\vec{r} - \vec{r}_0(t')|$. At the moment of observation, t, all light dots emitted at some retarded moment of time t' form a sphere with radius $c(t - t')$ and center $\vec{r}_0(t')$. Such spheres (hereinafter referred to as "light spheres") created for a given t at different retarded instants t' are nested within each other without intersecting because the velocity of the charge is always less than the speed of light. Figure 1 shows sections of light spheres in the plane of a charged particle moving in a circle with a speed of $0.8c$. It also shows lines connecting light dots emitted along the tangents to the trajectory (Fig. 1(a)) and along the radii directed to the corresponding retarded positions (Fig. 1(b)).

The variation of $\vec{n}$ with respect to the retarded time t' defines a curve in space that begins at $\vec{r}_0(t)$. Electric field lines were constructed from such a parametrization in the 1980s.[5–8] The differential equations defining electric field lines, after a remarkable transformation, reduce to linear differential equations with variable coefficients. These coefficients depend on one parameter $b = \varsigma/\gamma\kappa$ (where ς is the torsion of the trajectory, κ is the curvature of the trajectory, and γ is the Lorentz factor of the particle). If the value of b is constant, these equations are differential equations with constant coefficients.

In this paper, we derive these equations and their general analytic solution. The class of trajectories with constant b includes all planar trajectories ($\varsigma = 0$). We exploit this fact to construct the electric field lines of a charge moving in an

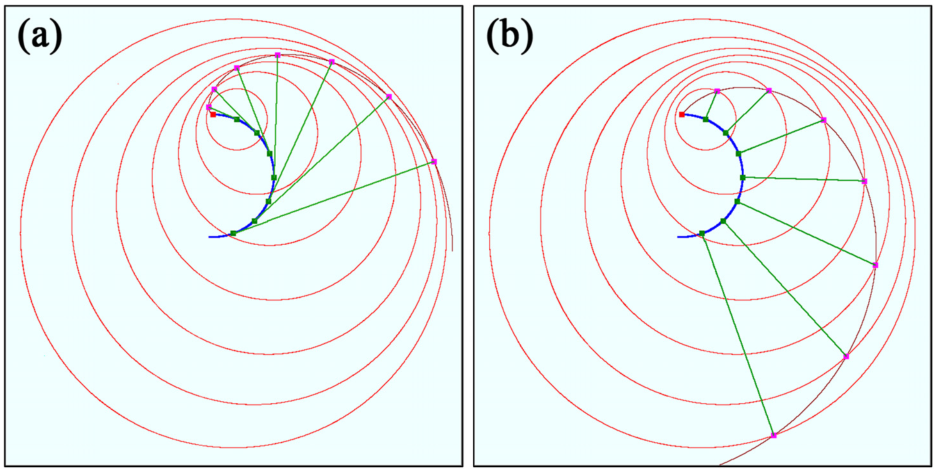

Fig. 1. A charged particle moves in a semi-circle with a speed of $0.8c$. (The trajectory is marked in blue, and the direction of motion is from bottom to top.) The red lines are cross sections of seven light spheres, which are formed by the light dots emitted at retarded moments of time. The corresponding retarded positions of the particle on the trajectory, centers of light spheres, are marked by green squares. (a) The line formed by the light dots emitted in the particle's direction of motion is marked in dark red. The magenta squares indicate the positions of these dots on the corresponding light spheres; the trajectories of the light dots are drawn in green. (b) The same as (a), except the light dots emitted along the radii directed to the corresponding retarded positions of the particle are shown.

electromagnetic plane wave, including the construction and visualization of three-dimensional field lines outside the orbital plane.

II. ELECTROMAGNETIC FIELD LINES OF AN ARBITRARILY MOVING CHARGE

The electric field $\vec{E}$ of an arbitrarily moving charged particle at time t is[2]

$$\vec{E} = -\frac{e}{R^2\gamma^2\left(1-(\vec{n}\cdot\vec{\beta})\right)^3} \times \left\{\vec{\beta} - \vec{n} - R\gamma^2\left[\vec{n}\times\left[(\vec{n}-\vec{\beta})\times\frac{d\vec{\beta}}{cdt'}\right]\right]\right\}, \quad (2)$$

where $R = |\vec{r} - \vec{r}_0(t')|$, $\vec{\beta}c = d\vec{r}_0(t')/dt'$, $\beta = |\vec{\beta}|$, and $\gamma = 1/\sqrt{1-\beta^2}$ is the Lorentz factor of the charged particle. The time t' is defined by Eq. (1). As noted above, the variation in $\vec{n}$ with respect to the retarded time t' determines the field lines.

A trajectory with several retarding points (**R**) and corresponding observation points (**P**) at the time of observation is shown in Fig. 2.

The field at any observation point is determined by a single retarded position defined by Eq. (1). The equation yielding the retarded position of the particle for a given observation point $\vec{r}$ and an arbitrary trajectory $\vec{r}_0(t)$ is a transcendental algebraic equation that cannot be solved analytically, in general. On the other hand, the variation of the unit vector $\vec{n}$ with respect to the retarded time defines a curve in space that begins at $\vec{r}_0(t')$,

$$\vec{L}(t') = \vec{r}_0(t') + c(t-t')\vec{n}(t'). \quad (3)$$

Equation (3) defines the geometrical locus of light dots at time t, which were emitted from the trajectory at instant t' in the direction of the vector $\vec{n}(t')$. Using this parametrization, the retardation equation may be solved by construction: $\vec{r} = \vec{L}(t')$. Equation (1) imposes a condition on the magnitude of $\vec{n}(t')$, but not its direction. Any curve defined by Eq. (3) penetrates all light spheres originating at $\vec{r}_0(t')$, and Eq. (2) implies that electric field lines have the property $\vec{n}\cdot\vec{E} = e/(R\gamma(1-(\vec{n}\cdot\vec{\beta}))^2 > 0$ everywhere. Therefore, Eq. (3) is suitable for finding field lines, as long as we can find functions $\vec{n}(t')$ such that the tangent to $\vec{L}(t')$ coincides with the direction of the electric field at each point.

The tangent to the curve defined by Eq. (3) at time t' is

$$\frac{d\vec{L}}{cdt'} = \vec{\beta} - \vec{n} + (t-t')\frac{d\vec{n}}{dt'}. \quad (4)$$

Requiring this to be parallel to the electric field in Eq. (2), we obtain a differential equation for $\vec{n}(t')$,

$$\frac{d\vec{n}}{dt'} = -\gamma^2\left[\vec{n}\times\left[(\vec{n}-\vec{\beta})\times\frac{d\vec{\beta}}{dt'}\right]\right]. \quad (5)$$

It is convenient to rewrite Eq. (5) in the Frenet–Serret frame, which describes the geometric properties of the curve itself

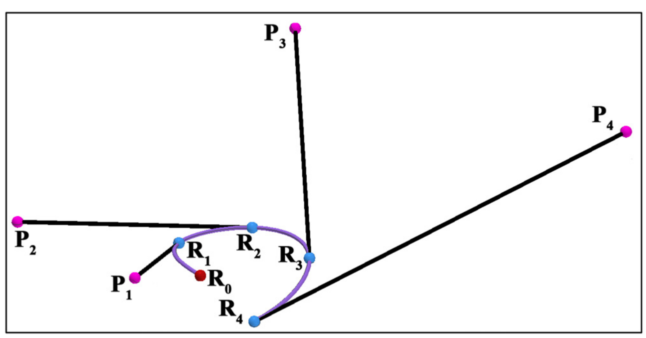

Fig. 2. Particle trajectory in the laboratory coordinate system is drawn in violet. At the observation time, the particle is at the point $\mathbf{R_0}$ (red sphere). The retarded positions of the particle ($\mathbf{R_1}$, $\mathbf{R_2}$, $\mathbf{R_3}$, $\mathbf{R_4}$, and cyan) are connected to the corresponding observation points ($\mathbf{P_1}$, $\mathbf{P_2}$, $\mathbf{P_3}$, $\mathbf{P_4}$, and magenta) by trajectories of light dots propagating in the direction of particle's velocity at retarded instants (black straight lines).

(the particle trajectory).[9] In this frame, the following unit vectors are introduced: the unit vector $\vec{e}_2$ tangent to the curve, the unit vector $\vec{e}_1$ directed opposite to the normal of the curve, and the binormal unit vector $\vec{e}_3 = [\vec{e}_1 \times \vec{e}_2]$. Frenet–Serret frames at several points of a trefoil trajectory are shown in Fig. 3. This trajectory has a significant curvature and torsion.[10]

In this coordinate system, we write

$$\vec{n} = n_1\vec{e}_1 + n_2\vec{e}_2 + n_3\vec{e}_3. \tag{6}$$

Using the Frenet–Serret derivations[9] of the tangent, normal, and binormal unit vectors with respect to the arc length, we reduce Eq. (5) to the following component equations:

$$\frac{dn_1}{cdt'} = \beta\gamma^2\kappa n_2 - \beta\varsigma n_3 - \beta^2\gamma^2\kappa(1-n_1^2) - \frac{d\beta}{cdt'}\gamma^2 n_1 n_2, \tag{7}$$

$$\frac{dn_2}{cdt'} = -\beta\gamma^2\kappa n_1 + \beta^2\gamma^2\kappa n_1 n_2 + \frac{d\beta}{cdt'}\gamma^2(1-n_2^2), \tag{8}$$

$$\frac{dn_3}{cdt'} = +\beta\varsigma n_1 + \beta^2\gamma^2\kappa n_1 n_3 - \frac{d\beta}{cdt'}\gamma^2 n_2 n_3. \tag{9}$$

These equations for electric field lines were obtained in Refs. 5 and 6.

To solve Eqs. (7)–(9), we use a Lorentz transformation. If $\vec{\nu}c$ is the velocity of the light dot in the reference frame of the particle and $\vec{n}c$ is its velocity in the laboratory frame, then

$$\vec{n}(t') = \frac{\vec{\beta}\left(1+\left(\left(\vec{\beta}\cdot\vec{\nu}(t')\right)(1-\gamma^{-1})/\beta^2\right)\right)+\vec{\nu}(t')\gamma^{-1}}{1+\left(\vec{\beta}\cdot\vec{\nu}(t')\right)}. \tag{10}$$

The transformation (10) for solving the equations of electric field lines was first applied in Ref. 7.

Substituting transformation (10) in Eqs. (7)–(9), we obtain the following vector equation for $\vec{\nu}(t')$:[11]

$$\frac{d\vec{\nu}}{dt'} = -\frac{\gamma-1}{\beta^2}\left[\left[\vec{\beta}\times\frac{d\vec{\beta}}{dt'}\right]\times\vec{\nu}\right]. \tag{11}$$

Equation (11) describes the rotation of the vector $\vec{\nu}$ in the laboratory frame of reference with angular velocity

$$\vec{\Omega} = -\frac{\gamma-1}{\beta^2}\left[\vec{\beta}\times\frac{d\vec{\beta}}{dt'}\right]. \tag{12}$$

This value coincides with the angular velocity of Thomas precession (see, for example, Refs. 12–14). Thomas precession has a purely kinematic origin. It represents an observation in the laboratory coordinate system of a vector $\vec{\nu}$ that is bound to the particle in the instantaneous rest frame of the particle.

It is also evident that for rectilinear motion, the vectors $\vec{\beta}$ and $d\vec{\beta}/dt'$ are parallel, such that the right-hand side of Eq. (11) is zero. In this case, the functions $\vec{\nu}$ become constant, and this case corresponds to the results of Ref. 1.

Let us solve vector equation (11) by introducing a change of variables

$$d\varphi = c\beta\gamma\kappa dt'. \tag{13}$$

Equation (11) can now be rewritten as a system of equations as follows:

$$\frac{d\nu_1}{d\varphi} = \nu_2 - b(\varphi)\nu_3, \tag{14}$$

$$\frac{d\nu_2}{d\varphi} = -\nu_1, \tag{15}$$

$$\frac{d\nu_3}{d\varphi} = b(\varphi)\nu_1, \tag{16}$$

where

$$b(\varphi) = \varsigma(\varphi)/\gamma(\varphi)\kappa(\varphi) \tag{17}$$

is a known function of φ for a given trajectory. Thus, Eqs. (14)–(16) represent a system of homogeneous linear differential equations with variable coefficients. In general, such equations can be solved numerically, for example, by the method of successive approximations.[15]

Equations (14)–(16) have an integral of the motion: $\nu_1^2+\nu_2^2+\nu_3^2 = \text{const}$. (The constant should be set equal to unity to ensure $|\vec{\nu}| = 1$ and $|\vec{n}| = 1$.)

Let us analyze Eqs. (14)–(16) for the case of $b(\varphi) = \text{const}$. The formula defining $b(\varphi)$ contains the torsion of the trajectory $\varsigma(\varphi)$ in the numerator. Thus, for all planar trajectories, $\varsigma = 0$ and $b = 0$. An example of a trajectory with constant $b(\varphi)$ is a particle moving around a helix with constant speed: The torsion, curvature, and Lorentz factor are constant.

When b is constant, Eqs. (14)–(16) are reduced to a system of linear homogeneous equations with constant coefficients, which can be solved easily as follows:[16,17]

$$\nu_1 = H\sqrt{1+b^2}\sin\left(\sqrt{1+b^2}(\varphi-\varphi_0)\right), \tag{18}$$

$$\nu_2 = H\cos\left(\sqrt{1+b^2}(\varphi-\varphi_0)\right) \pm b\sqrt{1/(1+b^2)-H^2}, \tag{19}$$

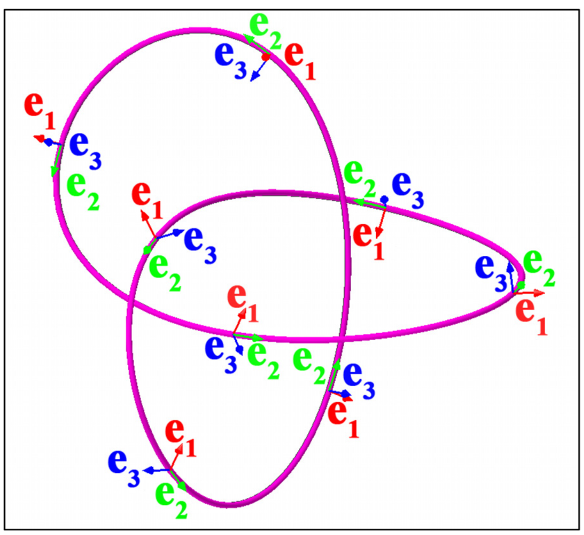

Fig. 3. Vectors of the Frenet–Serret frames at several points of the trefoil trajectory. The red vectors are directed along $\vec{e}_1$ (opposite to the normal), the green vectors are directed along $\vec{e}_2$ (tangent), and the blue vectors are directed along $\vec{e}_3$ (binormal).

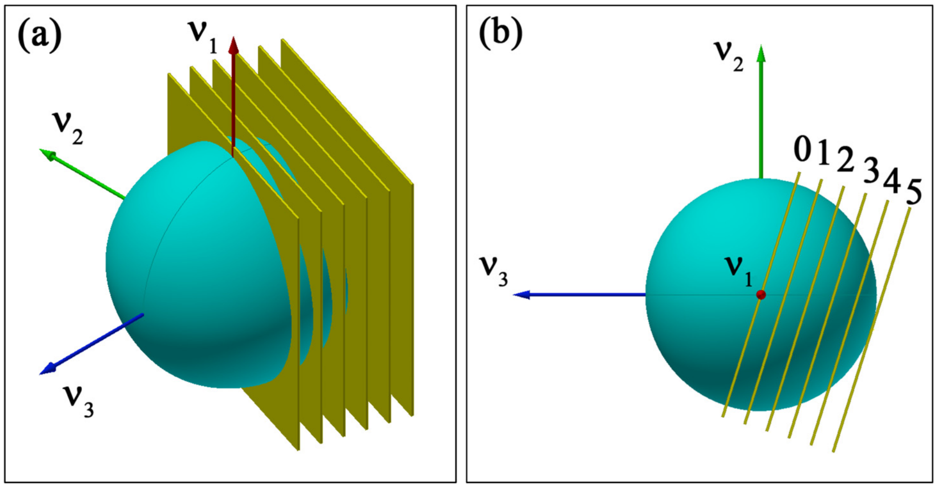

Fig. 4. Unit sphere cut by planes $b\nu_2 + \nu_3 = const$. (a) 3D view. (b) View in the (ν_2, ν_3) plane. The numbers 0, 1, 2, 3, 4, and 5 label several values of the constant H in Eq. (21). The plane 5 corresponds to $H = 0$ and touches the sphere.

$$\nu_3 = -bH\cos\left(\sqrt{1+b^2}(\varphi - \varphi_0)\right) \pm \sqrt{1/(1+b^2) - H^2}. \tag{20}$$

The solutions depend on two integration constants φ_0 and H (φ_0 varies within $(0,\ 2\pi)$, and H varies within $(0,\ 1/\sqrt{1+b^2})$).

When b is constant, Eqs. (15) and (16) yield another integral of the motion as follows:

$$b\nu_2 + \nu_3 = \pm\sqrt{1+b^2}\sqrt{1 - H^2(1+b^2)}. \tag{21}$$

Equation (21) defines a set of straight lines in the (ν_2, ν_3) plane that are parallel to the line $b\nu_2 + \nu_3 = 0$. This line corresponds to the condition $H = 1/\sqrt{1+b^2}$. The lines of the electric field correspond to the motion of a point along circles in the space (ν_1, ν_2, ν_3). These circles are defined by the intersection of the unit sphere having its center at the origin with the set of planes defined by Eq. (21). The condition $H = 1/\sqrt{1+b^2}$ corresponds to a great circle of the sphere, and when $H = 0$, the planes touch the unit sphere at the opposite ends of a diameter (see Fig. 4).

For the class of arbitrary planar trajectories,

$$\nu_3 = \pm\sqrt{1 - H^2} = \text{const}. \tag{22}$$

The class of electric field lines in the plane of motion of the particle is defined by $H = 1$. Equations (18)–(20) become

$$\nu_1 = \sin(\varphi - \varphi_0), \tag{23}$$

$$\nu_2 = \cos(\varphi - \varphi_0). \tag{24}$$

To summarize, we construct each electric field line as follows: First, for a given particle trajectory, the velocity, Lorentz factor, curvature, and torsion are computed. (For planar trajectories, the torsion is zero.) Next, φ is computed using Eq. (13). Then, $b(\varphi)$ is computed using Eq. (17). (This vanishes for planar trajectories.) Next, $\vec{v}(t')$ is computed by solving Eqs. (14)–(16) or Eqs. (23) and(24) for planar motion. The Lorentz transformation in Eq. (10) is used to find $\vec{n}(t')$. Finally, the field line is constructed using Eq. (3).

III. ELECTRIC FIELD LINES OF A CHARGE MOVING IN A LINEARLY POLARIZED PLANE WAVE

Let us consider the electric field lines of a charged particle moving in a linearly polarized plane wave. We will compare the field with synchrotron radiation and the radiation from linear oscillation in the appropriate limits.

A. Trajectory of a particle

The trajectory of a charged particle in a plane monochromatic linearly polarized wave is solved in a general form (see, e.g., Ref. 2). The electric field $\vec{E}$ in the wave is chosen in the direction of the axis Y: $E_y = E\cos(\omega(t - x/c))$, and the wave propagates in the direction of the axis X. In a reference frame in which the particle is at rest on the average, the parametric representation of motion is written in the following form:

$$x = -\frac{e^2E^2c}{8\Gamma^2\omega^3}\sin 2\eta, \tag{25}$$

$$y = -\frac{eEc}{\Gamma\omega^2}\cos\eta, \tag{26}$$

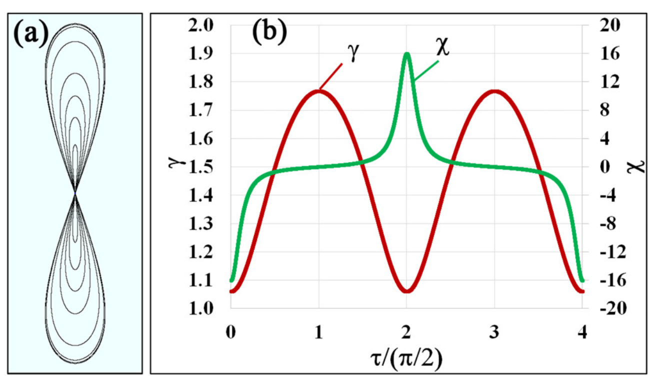

Fig. 5. (a) Figure eight trajectories for different α: 0.3 for the innermost trajectory, and 0.5; 0.7; 1; 2; and 5 moving outward. For $\alpha > 10$, trajectories practically coincide. (b) Dependence of Lorentz factor γ and scaled curvature χ on scaled time for $\alpha = 1$.

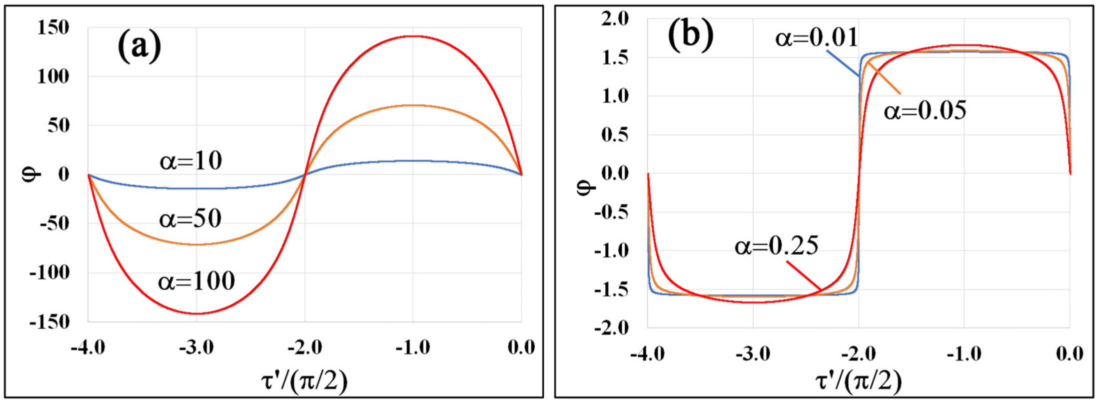

Fig. 6. Plots of $\varphi(\tau')$ for (a) large values of α: 100, 50, and 10 and (b) small values of α: 0.25, 0.05, and 0.01 (the observation time is set as zero).

$$z = 0, \tag{27}$$

$$t = \frac{\eta}{\omega} - \frac{e^2E^2}{8\Gamma^2\omega^3}\sin 2\eta, \tag{28}$$

where ω is the frequency of the wave, $\eta = \omega(t - x/c)$ is the wave phase, and $\Gamma^2 = m^2c^2 + (e^2E^2/2\omega^2)$ (m is the mass, and e is the charge of the particle). Equations (25)–(28) define planar trajectories, so Eqs. (23) and (24) can be used to construct field lines.

To simplify the representation of the trajectory, we introduce the following dimensionless parameters: $\xi_x = x/\hat{\lambda}$, $\xi_y = y/\hat{\lambda}$, and $\tau = \omega t$, where $\hat{\lambda} = c/\omega$. Let us also introduce a dimensionless parameter characterizing the wave

$$\alpha = \frac{eE}{\sqrt{2}mc\omega} = \frac{eE\hat{\lambda}}{\sqrt{2}mc^2} = \frac{1}{\sqrt{2}}\left(\frac{E}{E_0}\right)\frac{\hat{\lambda}}{r_0}, \tag{29}$$

where $E_0 = e/r_0^2 = 1.813\,393 \times 10^{18}$ V/cm, and $r_0 = e^2/mc^2 = 2.817\,940\,326\,2 \times 10^{-15}$ m is the classical radius of an electron. The physical interpretation of Eq. (29) is the ratio of the work done by the electric field of the wave over distances of the order of a wavelength to the rest energy of the charged particle. Hence, Eqs. (25)–(28) become

$$\xi_x = -\frac{\alpha^2}{4(1+\alpha^2)}\sin 2\eta, \tag{30}$$

$$\xi_y = -\frac{\sqrt{2}\alpha}{\sqrt{1+\alpha^2}}\cos\eta, \tag{31}$$

$$\tau = \eta - \frac{\alpha^2}{4(1+\alpha^2)}\sin 2\eta. \tag{32}$$

Equations (30)–(32) describe a characteristic figure eight motion because the frequency of motion along the axis X is twice the frequency along the axis Y. The characteristic features of the trajectories are determined by a single parameter α.

The size of the trajectory along the axis Y is proportional to α, and the size along the axis X is proportional to α^2; thus, for small values of α, the figure eight gradually approaches a straight line segment. For large values of α, the trajectory ceases to depend on α, tending to the limiting figure eight described by the formula $16\xi_x^2 + \xi_y^4 - 2\xi_y^2 = 0$. A set of trajectories for different α is shown in Fig. 5(a). The top points of the figure eight are passed at $\eta = \pi \pm 2\pi k, k = 0, \pm 1, \ldots$, and the center of the figure eight is passed at $\eta = \pi/2 \pm 2\pi k$, $k = 0, \pm 1, \ldots$. The outer figure eight corresponds to $\alpha = 100$. In this case, the value $\xi_y^{\max}$ is close to the limit value of $\sqrt{2}$. As the charge moves along the figure eight, its velocity and acceleration change, and the highest speeds are reached at the center (Fig. 5(b) for $\alpha = 1$). Figure 5(b) shows plots of the particle's Lorentz factor and normalized curvature of the

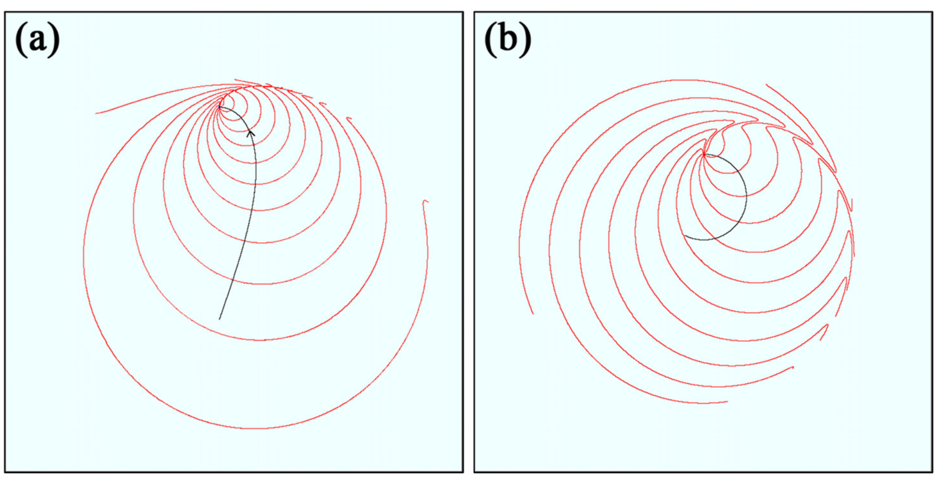

Fig. 7. Comparison of (a) the field lines for a charged particle moving in the field of a plane wave with $\alpha = 5$ and (b) synchrotron radiation for a charged particle moving along the circle contiguous to the trajectory in (a) at $\tau = 0$ with speed $\beta = 0.926$.

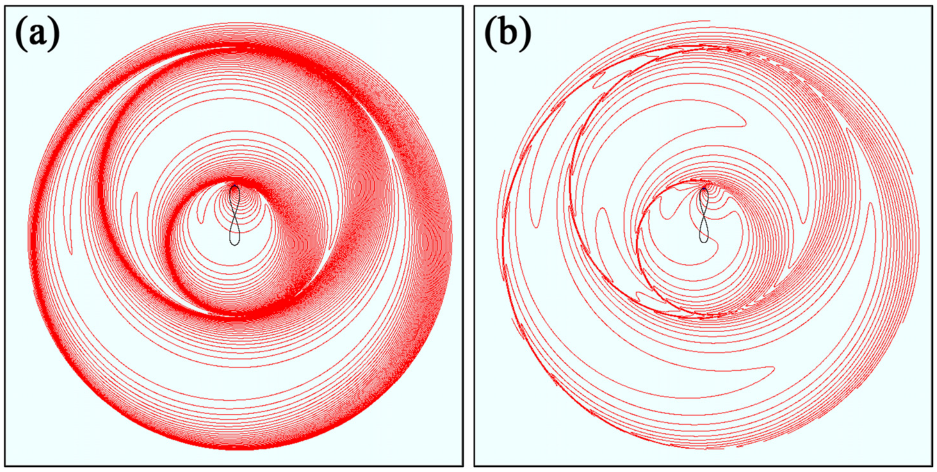

Fig. 8. Electric field lines for (a) $\alpha = 5$ and (b) $\alpha = 2$. The trajectory (figure eight) is represented in black. At the moment of observation, the particle is at the top of the figure eight and is moving from right to left.

trajectory $\chi = \hat{\lambda}\kappa$, which is maximum at the top points of the figure eight and changes sign while crossing the center.

As the trajectories described by Eqs. (25)–(28) are flat, expressions (23) and (24) can be used to construct electric field lines in the same plane. Multiple field lines may be constructed by changing the retarded time parameter $t' \leq t$ and computing φ using Eq. (13),

$$\varphi = c\int_t^{t'} \beta\gamma\kappa dt'' = \int_\tau^{\tau'} \beta\gamma\chi d\tau''. \tag{33}$$

Here, the integration variable is marked with double prime.

Figure 6 shows several plots of function φ with respect to the retarded time for different values of α.

It is evident that for large α (Fig. 6(a)), within one period of the charge reversal on the figure eight, the parameter φ also reaches large values, which corresponds to the fact that in Eqs. (23) and (24), the trigonometric functions make many revolutions. As $\alpha \to 0$ (Fig. 6(b)), the function φ tends to a characteristic meander between two values: $\pi/2$ for $-\pi < \tau' < 0$ and $-\pi/2$ for $-2\pi < \tau' < -\pi$. "Jumps" occur from one value to another when the retarded time is a multiple of π. In this case, the trajectory approaches that of linear oscillation.

It is interesting to estimate the maximum value of the parameter α for charged particles moving in existing laser waves. Studies on laser acceleration are nowadays at the forefront of research in physics (see, for example, Refs. 18 and 19). Extreme laser field intensities allow the exploration of novel physical phenomena,[20] and relativistic laser–plasma interactions open the possibility of laser-driven particle accelerators.[21] For example, the Center for Relativistic Laser Science (CoReLS) uses a 4-PW femtosecond, ultrahigh power Ti: sapphire laser, based on the chirped pulse amplification (CPA) technique.[22,23] The laser field intensity of 10^{23} W/cm^2 corresponds to an electric field strength on the order of 8.7×10^{12} V/cm. For a wavelength of 800 nm, this leads to $\alpha = 153$ and $\gamma \sim 229$, i.e., in such a field, the motion of the charged particle is highly relativistic.

B. Field lines in orbit plane

The figures that follow were constructed using the application in the supplementary online material.[24]

First, we draw lines near the section of the trajectory corresponding to the observation time $\tau = 0$ for the parameter $\alpha = 5$. In Fig. 7, we compare the field lines of the figure eight with the synchrotron radiation field of a particle moving

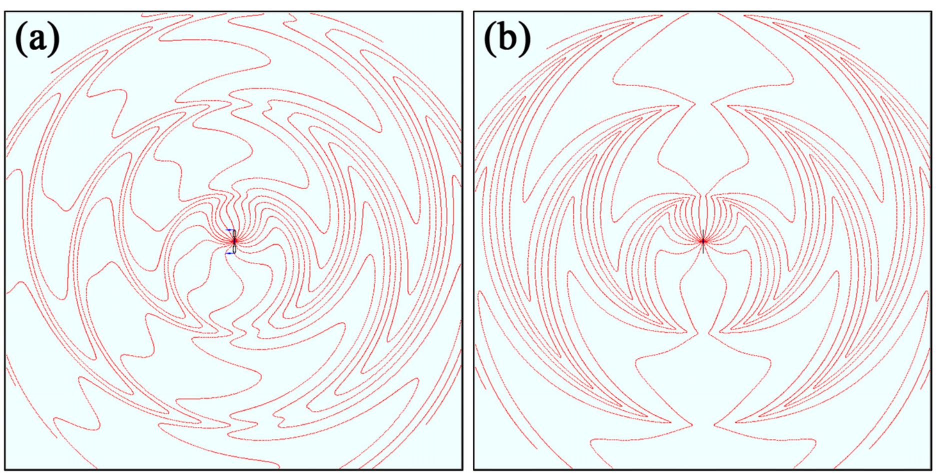

Fig. 9. (a) Electric field lines for a figure eight trajectory. Blue arrows show the direction of the particle's velocity at the extreme points of the trajectory. (b) Electric field lines for linear oscillation. For (a) and (b), $\alpha = 0.685\,994\,341$ ($\beta_{max} = 0.8$).

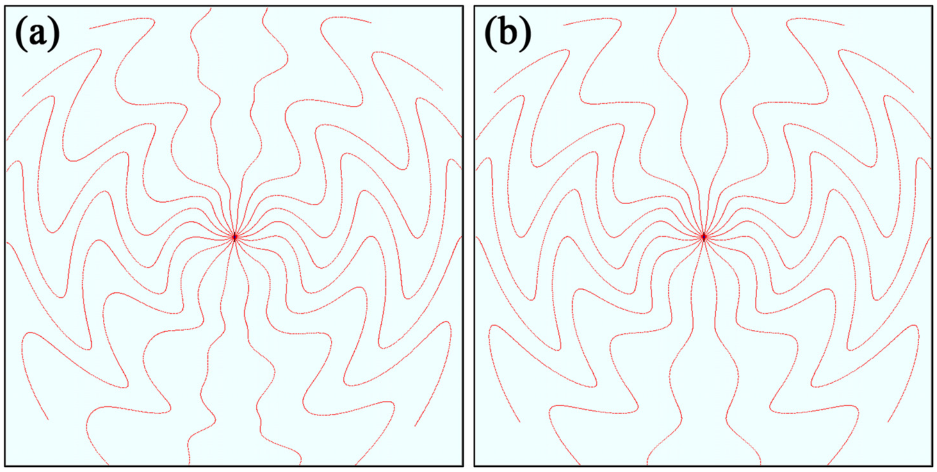

Fig. 10. Electric field lines for (a) the figure eight and (b) linear oscillation when $\alpha = 0.25$.

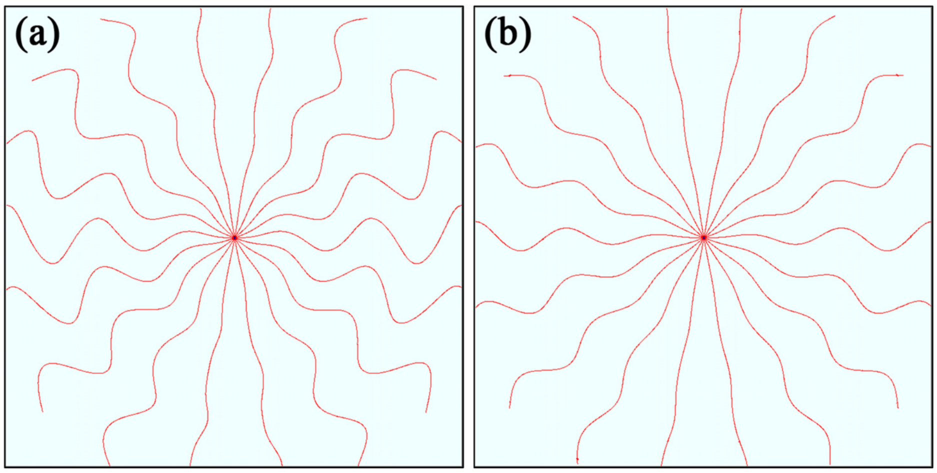

Fig. 11. Electric field lines for the figure eight for (a) $\alpha = 0.1$ and (b) $\alpha = 0.05$.

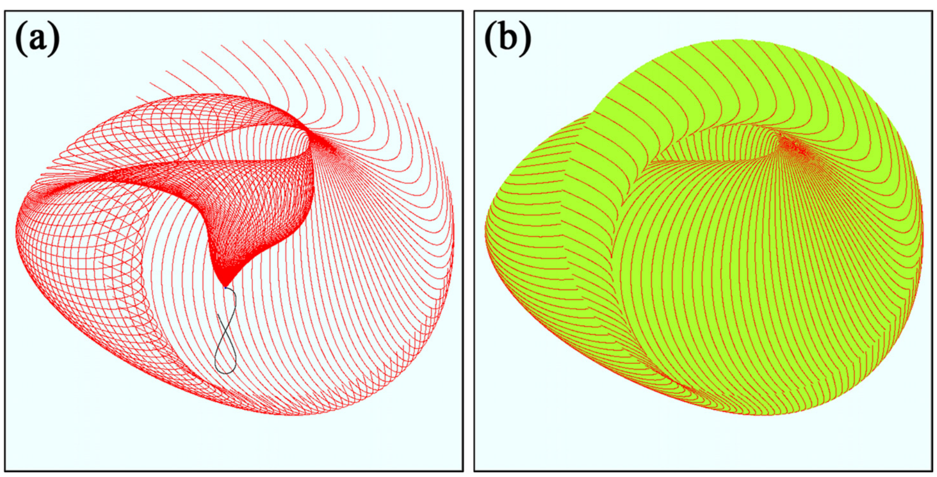

Fig. 12. The surface $H = 0.6$ ($\theta = 60^\circ$). (a) 90 electric field lines and trajectory without elimination of hidden fragments of the surface. (b) The same 90 lines are depicted using the Z-buffer algorithm, by which hidden areas of the surface are eliminated.

around a circle contiguous to the figure eight trajectory at $\tau = 0$. The radius of the circle is 0.167, and the speed of the particle is $\beta = 0.926$.

Figure 7 shows that the structure of the field lines for the figure eight motion is similar to synchrotron radiation in the region close to the charge position.

For values $\alpha = 5$ and 2, the field lines are presented over a larger region in Fig. 8.

In both cases, the number of lines depicted is 18 and they correspond to a uniform distribution of the initial parameter φ_0 from 0 to 2π. The denser filling at (a) indicates that at larger values of α, the trigonometric functions (23) and (24) make more turns around the particle, as indicated by Fig. 6(a).

At small α, the trajectory approaches a straight line segment along which the charge oscillates sinusoidally. This case of rectilinear motion was analyzed in Ref. 1. In Fig. 9, we compare the field patterns of figure eight and rectilinear motions. We model the motion along a straight line segment by the following equation:

$$\xi_y = -\frac{\sqrt{2}\alpha}{\sqrt{1+\alpha^2}}\cos\tau, \tag{34}$$

(see Eqs. (30)–(32) with $\xi_x = 0$ and $\tau = \eta$).

The maximum velocity when the charge moves along the figure eight is reached at the center, which corresponds to the value $\eta = \pi/2$. The value $\beta = 0.8$ is reached at $\alpha = 0.685\,994\,341$.

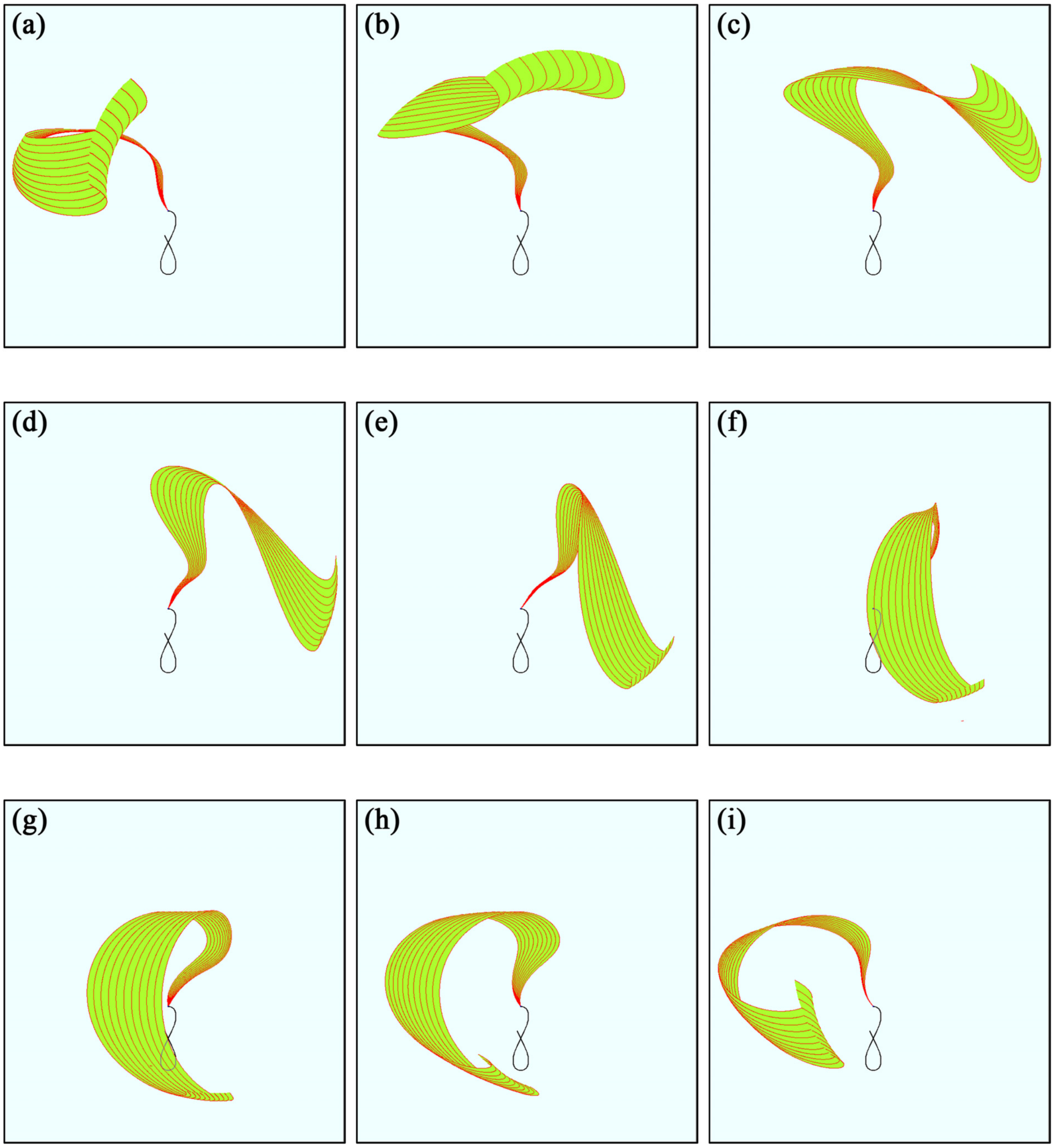

Fig. 13. The nine surface areas corresponding to the parameter $H = 0.6$ ($\theta = 60^\circ$) are presented. The ranges of the parameter φ_0: (a) $(0, 2\pi/9)$; (b) $(2\pi/9, 4\pi/9)$; (c) $(4\pi/9, 6\pi/9)$; (d) $(6\pi/9, 8\pi/9)$; (e) $(8\pi/9, 10\pi/9)$; (f) $(10\pi/9, 12\pi/9)$; (g) $(12\pi/9, 14\pi/9)$; (h) $(14\pi/9, 16\pi/9)$; and (i) $(16\pi/9, 2\pi)$ are chosen such that the whole surface is eventually filled. The trajectory of the particle is shown in black.

A certain similarity is apparent in the images in Fig. 9, especially in the area near the charge. The field lines of the figure eight are asymmetric relative to the vertical axis. This is because at the top and bottom of the figure eight, the charge has horizontal components of velocity, which are in the same direction.

In Fig. 10, the electric field lines for the figure eight and linear oscillation are compared for $\alpha = 0.25$. The difference is observable, but is significantly smaller than that in Fig. 9.

For smaller values of α, the electric field lines for the figure eight and linear oscillation practically coincide. Figure 11 shows only lines for the figure eight for $\alpha = 0.1$ and $\alpha = 0.05$. It is evident that the field lines along the vertical axis are less wavy than in the horizontal direction. This corresponds to Thomson scattering[25] when the maximum dipole radiation is observed in the plane orthogonal to the dipole axis.

C. Field lines outside the orbital plane

In the case of nonplanar trajectories, all field lines have a 3D characteristic.[26] The electric field lines have a rather complex structure and form complicated surfaces.

Figure 12(a) shows a surface of lines for a charge with parameter $\alpha = 1$ and constant $H = 0.3$. The image plane (X_{SC}, Y_{SC}) is rotated with respect to the plane (X, Y) of the laboratory coordinate system by an angle 60° about the X axis. The surface is shaped with 90 lines corresponding to a uniform distribution of the constant φ_0 between 0 and 2π. The direct construction of field lines, without the analysis of the distance from sections of lines to the observer, does not present a clear picture of their locations in space. Caustics of the field can be observed, but the three-dimensional structure of the surface is difficult to identify, because the lines on hidden surfaces are plotted in Fig. 12(a). To eliminate these hidden surfaces, we used the Z-buffer or depth buffer method[27] in Fig. 12(b). The picture is now clearer, but it is difficult to see how the field is coupled to the trajectory of the particle.

In order to identify this structure with respect to the trajectory, we have drawn nine surfaces, each corresponding to a limited range of φ_0. Figure 13 shows the result for $H = 0.6$.

The results in this section are preliminary, as it is difficult to represent non-planar lines in three-dimensional space. However, research in this direction should be continued. In electrodynamics, there are many interesting problems in which the trajectories of motion are non-planar. One of the simplest cases is helical motion with nonzero constant b. The field lines can be computed analytically. The motion of charged particles in magnetic fields for high-temperature plasma confinement is more interesting, as the particles move in helices with a variable radius and pitch.[28] Similar problems arise in astrophysics.[29] The method of representing spatial field lines for planar motions developed in this study can be adapted for such non-planar trajectories.

IV. CONCLUSION

We have shown that the equations of electric field lines of an arbitrarily moving charge can be reduced to linear differential equations. These equations may be solved analytically in some cases, including any planar motion. Visualization of the field clearly indicates details of its structure, including the spatial concentration of radiation.

This method of determining the electric field lines can also be applied to construct magnetic field lines, which lie on the light spheres.[7] Another problem of interest is the development of Lorentz covariant system of field lines[30] and the determination of the electromagnetic field tensor by such lines.[31]

ACKNOWLEDGMENTS

The authors are grateful to one of the article reviewers who suggested the term "light dots" to describe the construction of field lines and also noted the equivalence of the basic electric field line equations [(11) and (12)] with the equation of Thomas precession. The authors are also grateful to A. G. Harutyunyan for his help in improving the quality of the figures. This research was supported by RA MES SCS in the frame of Project Nos. 20APP-2G001 and 21T-2G079. This research was also partly supported by the National Research Foundation (NRF) of Korea (Grant No. NRF2016R1A5A1013277).

AUTHOR DECLARATIONS

Conflict of Interest

The authors have no conflicts to disclose.

[a]ORCID: 0000-0002-1823-285X.
[b]ORCID: 0000-0001-7014-4120.

[1]D. Ruhlandt, S. Mühle, and J. Enderlein, "Electric field lines of relativistically moving point charges," Am. J. Phys. **88**(1), 5–10 (2020).

[2]L. D. Landau and E. M. Lifshitz, *The Classical Theory of Fields*, 3rd ed. (Pergamon, 1971), Chap. 8, p. 158.

[3]R. Fitzpatrick, *Maxwell's Equations and the Principles of Electromagnetism* (Infinty Science, 2008), Chap. 4.9, p. 137.

[4]J. H. Field, "Retarded electric and magnetic fields of a moving charge: Feynman's derivation of Lienard–Wiechert potentials revisited," arXiv:0704.1574v3 (2015).

[5]M. A. Aginian and S. G. Arutunian, "Force lines of electric and magnetic fields of arbitrary moving charge," Report No. EFI-684-74-83-YEREVAN (Yerevan Physics Institute, Yerevan, 1983).

[6]S. G. Arutyunyan, "Force lines of electric and magnetic fields of an arbitrarily moving charge," Radiophys. Quantum Electron. **28**(7), 619–624 (1985).

[7]S. G. Arutyunyan, "Electromagnetic field lines of a point charge moving arbitrarily in vacuum," Sov. Phys. Usp. **29**(11), 1053–1057 (1986).

[8]T. Shintake, "Real-time animation of synchrotron radiation," Nucl. Instrum. Methods Phys. Res., Sect. A **507**(1–2), 89–92 (2003).

[9]G. A. Korn and T. M. Korn, *Mathematical Handbook for Scientists and Engineers. Definitions, Theorems, and Formulas for Reference and Review* (Dover Publications, New York, 2000), Chap. 17.2–3, p. 567.

[10]The trefoil curve can be described parametrically using the phase ψ: $\vec{R}_{TRE} = (\sin\psi + 2\sin(2\psi),\ \cos\psi - 2\cos(2\psi),\ \sin 3\psi)$.

[11]In the derivation of (11), the Frenet–Serret relation of differentiation of the tangential vector along the trajectory is considered: $d\vec{\beta}/cdt' = (d\beta/cdt')\vec{e}_2 + \beta(d\vec{e}_2/cdt') = (d\beta/cdt')\vec{e}_2 - \beta^2\kappa\vec{e}_1$. The components of the vector equation (11) are the following: $d\nu_1/cdt' = \beta\gamma\kappa\nu_2 - \beta\varsigma\nu_3$, $d\nu_2/cdt' = -\beta\gamma\kappa\nu_1$, $d\nu_3/cdt' = \beta\varsigma\nu_1$.

[12]H. Goldstein, Ch Poole, and J. Safko, *Classical Mechanics*, 3rd ed. (Addison Wesley, 2002), Chap. 7.3, p. 285.

[13]G. B. Malykin, "Thomas precession: Correct and incorrect solutions," Phys.-Usp. **49**(8), 837–853 (2006).

[14]V. L. Telegdi and R. Winston, "A dynamical interpretation of the Thomas precession," Helv. Phys. Acta **33**, 249–252 (1960).

[15]M. Tenenbaum and H. Pollard, *Ordinary Differential Equations: An Elementary Textbook for Students of Mathematics, Engineering, and the Sciences* (Dover Publications, New York 1985), Chap. 3.9, p. 40.

[16]The characteristic equation of the system (14)–(16) is $\lambda(\lambda^2 + 1 + b^2) = 0$, with roots $\lambda_1 = 0, \quad \lambda_{2,3} = \pm i\sqrt{1+b^2}$.

[17]S. G. Arutunian, M. A. Aginian, A. V. Margaryan, E. G. Lazareva, and M. Chung, "Electric field lines of an arbitrarily moving charged particle," arXiv:2109.10792 (2021).

[18]M. Turner *et al.*, "Experimental observation of plasma wakefield growth driven by the seeded self-modulation of a proton bunch," Phys. Rev. Lett. **122**, 054801 (2019).

[19]E. Adli *et al.*, "Experimental observation of proton bunch modulation in a plasma at varying plasma densities," Phys. Rev. Lett. **122**, 054802 (2019).

[20]A. Di Piazza, C. Muller, K. Z. Hatsagortsyan, and C. H. Keitel, "Extremely high-intensity laser interactions with fundamental quantum systems," Rev. Mod. Phys. **84**(3), 1177–1228 (2012).

[21]V. B. Pathak, S. K. Lee, K. H. Pae, C. I. Hojbota, Ch. M. Kim, and Ch. H. Nam, "Strong field physics pursued with petawatt lasers," AAPPS Bull. **31**, 4 (2021).

[22]Jin Woo Yoon, Jae Hee Sung, Seong Ku Lee, Hwang Woon Lee, and Chang Hee Nam, "Ultra-high intensity lasers as tools for novel physics," J. Korean Phys. Soc. **81**(6), 562–569 (2022).

[23]Jin Woo Yoon, Yeong Gyu Kim, Il Woo Choi, Jae Hee Sung, Hwang Woon Lee, Seong Ku Lee, and Chang Hee Nam, "Realization of laser intensity over 10^{23} W/cm^2," Optica **8**(5), 630–635 (2021).

[24]See supplementary material (Visual Basic 10 Application) online for 3D Figures: https://drive.google.com/drive/folders/1_Y2eH6yTn-y6xZQAt4pNsk6zZJCJ8FOB?usp=share_link.

[25]E. S. Sarachik and G. T. Schappert, "Classical theory of the scattering of intense laser radiation by free electrons," Phys. Rev. D **1**(10), 2738–2753 (1970).

[26]It should be noted that an attempt to represent the electric field lines of synchrotron radiation in space was made in the preprint: S. G. Arutunian and M. R. Mailian, "Twelve illustrations of the synchrotron radiation field," Preprint YerPhI **1163**(40), 89 (1989).

[27]T. Theoharis, G. Papaioannou, N. Platis, and N. Patrikalakis, *Graphics & Visualization, Principles & Algorithms* (A.K. Peters, 2012), Chap. 5.5.1, p.160.

[28]A. V. Burdakov and V. V. Postupaev, "Multiple-mirror trap: A path from Budker magnetic mirrors to linear fusion reactor," Phys.-Usp. **61**(6), 582–600 (2018).

[29]T. G. Northrop, "Adiabatic theory of charged particle motion," in *Radiation Trapped in the Earth's Magnetic Field, Astrophysics and Space Science Library*, edited by B. M. McCormac, Vol 5 (Springer, Dordrecht, 1966).

[30]W. A. Newcomb, "Motion of magnetic lines of force," Ann. Phys. **3**(4), 347–385 (1958).

[31]S. G. Arutyunyan, "Equivalent representation of orthogonal-field electrodynamics by system of covariant lines of force, Izvestiya Vysshikh Uchebnykh Zavedenii," Radiofizika **35**(3), 313–323 (1992) [(Translated from Russian by Plenum Publishing Corporation, 1992)].

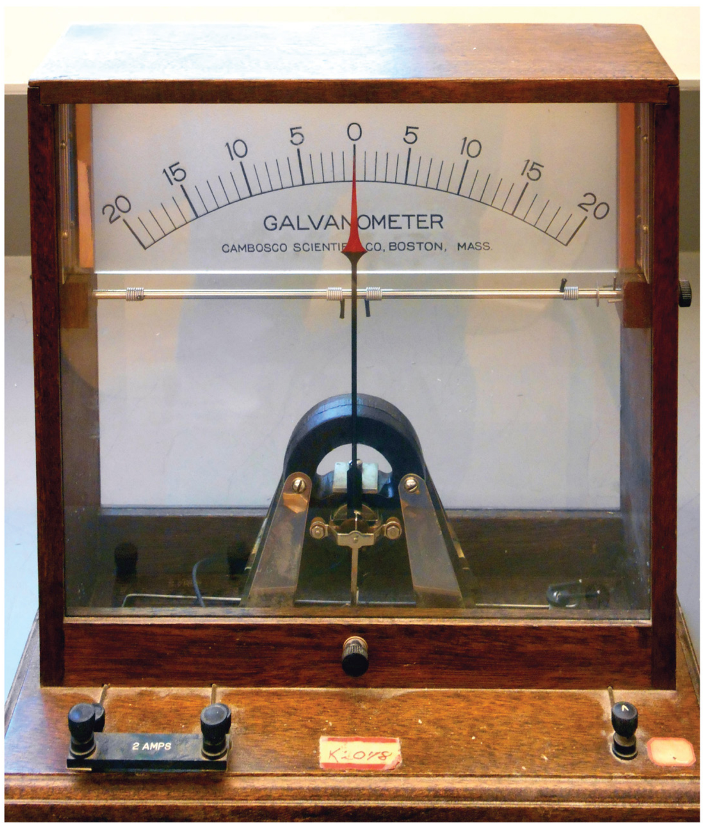

Lecture Table Galvanomete

You are unlikely to use a small lecture table galvanometer in the classroom, but recently I have discovered a new use for it in the undergraduate laboratory. Devices like this are resonant systems with free oscillation periods of the order of one second. When driven by a low-frequency voltage signal a resonance curve can be traced out, and Quality Factor (Q) determined. See: Thomas B. Greenslade, Jr., "Electro-Mechanical Resonance Curves:, Phys. Teach., 56, 144-145 (2018) The instrument was made by Cambosco of Boston in the 1930s and is at Mills College in Oakland, California. (Picture by David Keeports and text by Thomas B. Greenslade, Jr., Kenyon College)